Investigation of the Membrane Behavior of UD-NCF in Macroscopic Forming Simulations

Bastian Schäfer[1,a*], Stefan Haas[1,b], Philippe Boisse[2,c], Luise Kärger[1,d]

[1]Karlsruhe Institute of Technology (KIT), Institute of Vehicle System Technology (FAST), Germany

[2]Université de Lyon, LaMCoS CNRS, INSA-Lyon, F-69621, France

[a]bastian.schaefer@kit.edu, [b]stefan_haas97@t-online.de, [c]philippe.boisse@insa-lyon.fr, [d]luise.kaerger@kit.edu

Keywords: UD-NCF, Non-Orthogonal Material Modelling, FE-Forming Simulation, Process Simulation

Abstract. Unidirectional non-crimp fabrics (UD-NCF) provide an exceptionally high lightweight potential compared to other dry fabrics. However, their defect-free formability is limited compared to woven or biaxial fabrics due to their susceptibility to draping effects like wrinkling, gapping and fiber waviness. To predict these local effects and the global forming behavior efficiently, macroscopic modelling approaches require the consideration of the mesoscopic material structure. A very detailed macroscopic approach was proposed by Schirmaier et al. [1] and its prediction accuracy validated with qualitative and quantitative comparisons to component forming results. However, the approach couples several deformation modes and therefore requires a very high number of inversely determined material parameters. In the present work a new macroscopic forming model for the membrane behavior of UD-NCF is introduced based on superimposed shear, transverse tensile and perpendicular to the carbon fiber tows oriented compressive strains. The model is parametrized with experimental results of different off-axis-tension-tests (OATs) (30°, 45° and 60°) and compared to the model proposed by Schirmaier et al. [1]. The results of the new membrane model agree well with the experimental and simulative results in large areas, while utilizing a significantly reduced number of material parameters. However, some limitations are identified due to the reduced complexity of the model.

Introduction

Unidirectional non-crimp fabircs (UD-NCF) have straight fibres and therefore provide a higher lightweight potential compared to woven fabrics with undulated fibres. However, their formability is challenging and they are more susceptible to draping effects like wrinkling, gapping and fibre waviness due to their exclusively unidirectional high stiffness [2–4]. In order to predict these effects and the global forming behaviour efficiently, macroscopic modelling approaches can be used for complexly curved geometries. However, woven fabrics have so far mainly been the focus of research on macroscopic forming simulations [5,6] due to their better formability. In contrast, biaxial NCF [7–10] or UD-NCF [1,11–13] have been investigated much less and mostly based on mesoscopic approaches [11,12], which can only be used to a limited extent for component forming simulations due to their high numerical effort. Nevertheless, they can predict local forming effects, while macroscopic approaches only capture the deformations mechanisms occuring on the meso-scale in a homogenized manner to indicate areas with a high likelihood of e.g. waviness, gapping or compaction perpendicular to the carbon fibre bundles [14].

Krogh et al. [13] proposed a simple macroscopic model based on the built-in fabric material model in Abaqus to describe the membrane behaviour of quasi-unidirectional glass-fiber NCF. The model is parametrized based on experimental results of the 45°-Off-Axis-Tension-test (OAT), also called Bias-extension-test, and predicts the early force-displacment-relation well. However, the model overestimates the shear response for larger deformations as NCF deforms under more simple instead of pure shear. A very detailed macroscopic approach was proposed by Schirmaier et al. [1] to model large shear strains superimposed with large non-orthogonal tensile strains in the stitching direction and

compressive strains perpendicular to the carbon fiber tows. The material parameters were inversely determined based on 30°-, 45°- and 60°-Off-Axis-Tension-tests (OATs). Its prediction accuracy was validated with qualitative [1] and quantitative [14] comparisons to component forming results. However, the complex model requires a high number of material parameters to describe the membrane behavior under multiaxial loading conditions.

In this work, a new macroscopic forming model for the membrane behavior of UD-NCF is introduced based on superimposed shear, transverse tensile and perpendicular to the carbon fiber tows oriented compressive strains. The model is parametrized with experimental results of different OATs and compared to the model proposed by Schirmaier et al. [1]. The simplified model is used to identify the essential mechanisms as well as relevant couplings between different deformation modes and to determine unnecessary material parameters.

Macroscopic Modelling Approach for UD-NCF

The fibre yarns in UD-NCF are bonded together with a polymer stitching pattern and few glass fibres on the back to improve the handleability. Therefore, the deformation behaviour of UD-NCF differs considerably from woven fabrics which deform manly under pure shear due to the intrinsic cohesion of the interwoven yarns. Experimental tests of UD-NCF under multiaxial loading conditions in different OATs (30°, 45° and 60°) showed large shear strains superimposed with significant tensile deformations in the stitching direction and compression perpendicular to the carbon fibre bundles [3]. This deformation behaviour needs to be captured by the macroscopic modelling approach. Therefore, the constitutive equations of the membrane model proposed by Schirmaier et al [1] and the new model are outlined in the following. Both models were implemented as user subroutines (VUMAT) for the commercial FE-solver Abaqus, which require the stress in the co-rotational Green-Naghdi frame $\hat{\sigma}$.

Membrane model by Schirmaier et al. [1]. In this section only the key mechanisms of the membrane model relevant for this work are summarized. A comprehensive description can be found in [1,15]. The model consists of a non-orthogonal elastic-plastic material behaviour based on a custom linear strain measure ($\underline{\varepsilon}$) superimposed by an orthogonal compressive stress based on an introduced perpendicular strain component $\varepsilon_\perp$ (cf. Fig. 1a). The resulting material formulation uses the principle material strain ε_1 in fibre direction, the non-orthogonal transverse strain ε_2 contributing only under tensile loading in the stitching direction, the shear angle γ_{12} and the perpendicular strain $\varepsilon_\perp$ superimposed only for an in-plane compression. This approach yields a total co-rotational Cauchy stress $\hat{\sigma}$ consisting of a stress $\hat{\sigma}_{\mathrm{pm}}$ in principal material direction and a stress $\hat{\sigma}_\perp$ perpendicular to the fibre direction according to

$$\hat{\sigma} = \hat{\sigma}_{\mathrm{pm}}(\varepsilon_1, \varepsilon_2, \gamma_{12}) + \hat{\sigma}_\perp(\varepsilon_\perp, \gamma_{12}) \quad \text{with} \quad \hat{\sigma}_\perp = \mathbf{0} \ \text{ for } \ \varepsilon_\perp < 0. \tag{1}$$

Elastic-plastic behaviour is introduced by splitting the total tensile strain ε_2 and shear angle γ_{12} into elastic $(\cdot)_{,\mathrm{e}}$ and hardening plastic parts $(\cdot)_{,\mathrm{p}}$. A yield surface $R_{2,\Gamma}(\varepsilon_{2,\mathrm{p}}, \gamma_{12})$ and a yield curve $R_{12,\Gamma}(\gamma_{12,\mathrm{p}})$ define the transition from a purely elastic to an elastic-plastic deformation, thus coupling the transverse deformation to the total shear angle γ_{12}. The perpendicular compressive stress $\hat{\sigma}_\perp$ is additively superimposed with a nonlinear elastic material law depending on $\varepsilon_\perp$ and γ_{12}, to account for macroscopic wrinkling starting at higher perpendicular in-plane compression in the case of high shear angles. Therefore, the effective compressive stiffness is higher for small shear angles then in case of high shear angels [1]. The final membrane model requires a total of 49 material parameters and utilizes two different couplings between deformation modes.

New proposed macroscopic membrane model. In order to investigate which mechanisms and couplings within a membrane approach are necessary to model the behaviour of UD-NCF, a simplified macroscopic membrane model is proposed. A hyperelastic St.Venant-Kirchhoff material formulation [17] based on the Green-Lagrange strain $\boldsymbol{E}$ and the second Piola-Kichhoff stress $\boldsymbol{S}$ is applied, thus
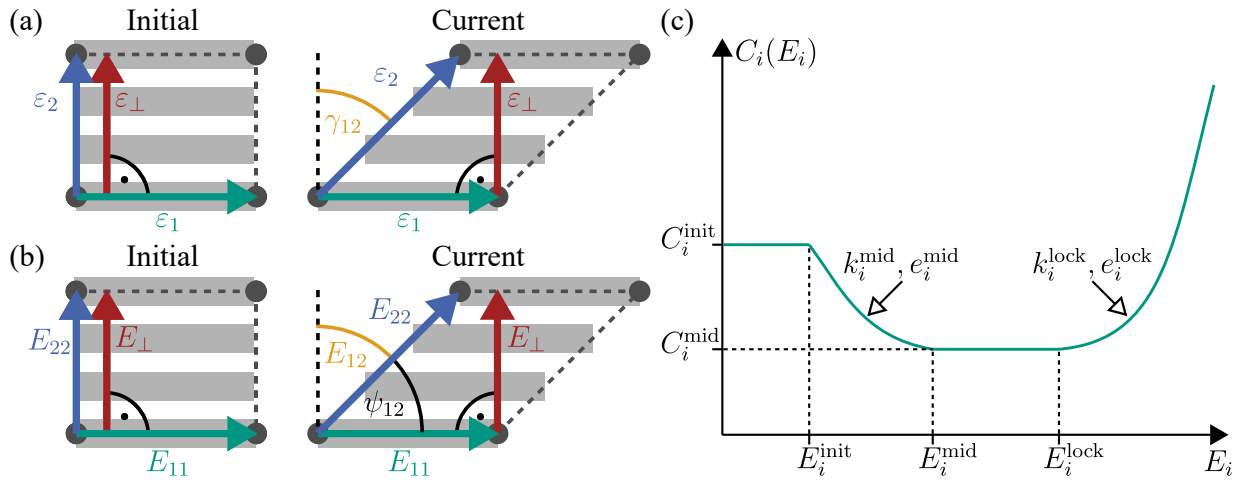
Fig. 1: Schematic illustration of the strain directions in the initial and current configuration of the membrane model (a) introduced by Schirmaier et al. [1] and (b) proposed in this work; (c) the model for the nonlinear stiffnesses utilizing 3 piecewise functions (based on [16])

intrinsically capturing rotations due to large shear between different strain components (cf. Fig. 1b). The material behaviour is assumed to be nonlinear elastic without any couplings, which results in the stress in principal material direction

$$\hat{\boldsymbol{\sigma}}_{\mathrm{pm}} = J^{-1}\, \boldsymbol{U}\, \boldsymbol{S}\, \boldsymbol{U} \quad \text{with} \quad \boldsymbol{S} = \mathbb{C} : \boldsymbol{E} \stackrel[\text{notation}]{\text{2D-Voigt}}{=} \begin{pmatrix} C_1 & 0 & 0 \\ 0 & C_2(E_{22}) & 0 \\ 0 & 0 & C_\gamma(E_{12}) \end{pmatrix} \begin{pmatrix} E_{11} \\ E_{22} \\ E_{12} \end{pmatrix}, \qquad (2)$$

where J is the Jacobian determinant of the deformation gradient $\boldsymbol{F}$, $\boldsymbol{U}$ the stretch tensor of the polar decomposition $\boldsymbol{F} = \boldsymbol{R}\, \boldsymbol{U}$ and $\mathbb{C}$ is the elasticity tensor. Additionally, similar to [1], a perpendicular stress $\hat{\boldsymbol{\sigma}}_\perp$ is superimposed based on the strain

$$E_\perp = \sqrt{2E_{22} + 1}\, \sin(\psi_{12}) - 1 \quad \text{with} \quad \psi_{12} = \arccos\left(\frac{C_{12}}{\sqrt{C_{11}}\sqrt{C_{22}}}\right), \qquad (3)$$

where $\boldsymbol{C}$ ist the right Cauchy-Green tensor. This results in the perpendicular stress

$$\hat{\boldsymbol{\sigma}}_\perp = \boldsymbol{R}^\mathsf{T} \left(\boldsymbol{R}_\perp{}^\mathsf{T} \begin{pmatrix} 0 & 0 \\ 0 & \frac{C_\perp(E_\perp)}{\sqrt{C_{11}}} \end{pmatrix} \boldsymbol{R}_\perp \right) \boldsymbol{R} \quad \text{with} \quad \boldsymbol{R}_\perp = \frac{1}{\sqrt{C_{11}}} \cdot \begin{pmatrix} F_{11} & -F_{21} \\ F_{21} & F_{11} \end{pmatrix}. \qquad (4)$$

The nonlinear stiffnesses $(C_2, C_\gamma, C_\perp)$ are modeled as functions of their respective strains $(E_{22}, E_{12}, E_\perp)$, cf. Figure 1c, according to

$$C_i(E_i) = \begin{cases} C_i^{\mathrm{init}} & , 0 \leq |E_i| \leq E_i^{\mathrm{init}} \\ k_i^{\mathrm{mid}}(|E_i - E_i^{\mathrm{mid}}|)^{e_i^{\mathrm{mid}}} + C_i^{\mathrm{mid}} & , E_i^{\mathrm{init}} < |E_i| \leq E_i^{\mathrm{mid}} \ \text{with}\ k_i^{\mathrm{mid}} = \frac{C_i^{\mathrm{init}} - C_i^{\mathrm{mid}}}{E_i^{\mathrm{init}} - E_i^{\mathrm{mid}}} \\ C_i^{\mathrm{mid}} & , E_i^{\mathrm{mid}} < |E_i| \leq E_i^{\mathrm{lock}} \\ k_i^{\mathrm{lock}}(|E_i - E_i^{\mathrm{lock}}|)^{e_i^{\mathrm{lock}}} + C_i^{\mathrm{mid}} & , E_i^{\mathrm{lock}} < |E_i|. \end{cases} \qquad (5)$$

The formulation was chosen based on its high adaptability with relative few, easy to interpret parameters [16]. It consists of an initial modulus C_i^{init}, which decreases to a middle modulus C_i^{mid} over a strain range from E_i^{init} to E_i^{mid} and increases again after E_i^{lock}. This approach requires a total of seven

material parameters for each stiffness with $i = [2, \gamma, \perp]$. Additionally, to ensure disjunction between the perpendicular compressive and transverse tensile behaviour in case of equal sign, the following auxiliary conditions are introduced:

$$C_\perp(E_\perp) = 0 \text{ for } E_\perp > 0 \quad \text{and} \quad C_2(E_{22}) = 0 \text{ for } E_{22} < 0. \tag{6}$$

In summary, the new membrane approach is based on similar superimposed stresses as the model proposed by Schirmaier et al. [1], but different strain measures (mostly quadratic instead of linear) are used, plasticity and couplings of deformation mechanisms are neglected and a simple approach for the nonlinear stiffnesses is introduced. Nevertheless, for a more straightforward comparison to the results in [1], the linear strain measures are additionally calculated and utilized during the evaluation.
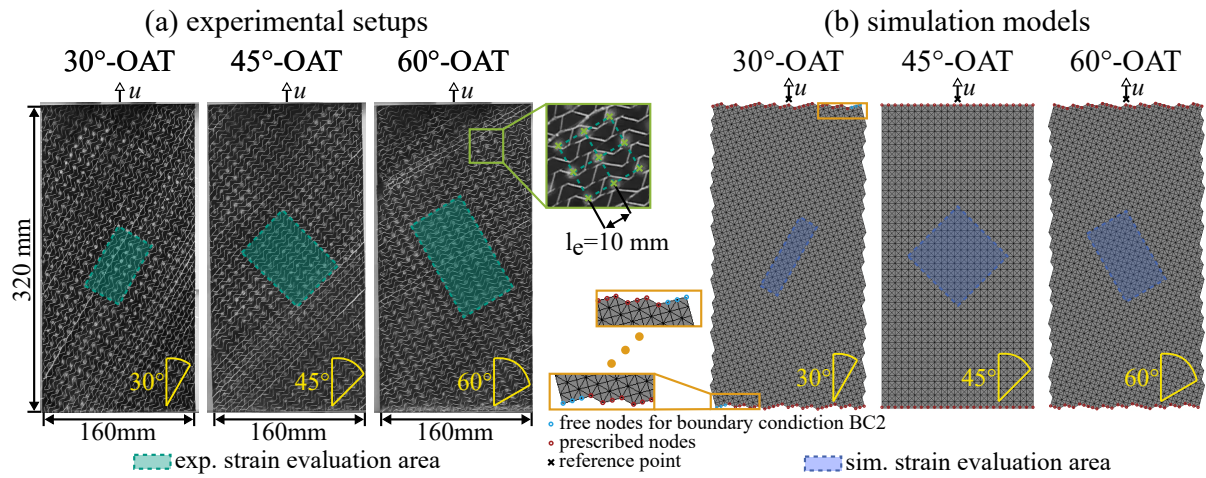

Fig. 2: (a) Experimental setups of the OATs with a square pattern of white points for optical measurements and highlighted areas (green) for an averaging of the strain components (based on [1]); (b) Simulation models with their respective boundary conditions to simulate slip in the clamping area during the 30°-OAT (boundary condition BC 2) and highlighted areas (blue) for an averaging of the strain components (based on [15])
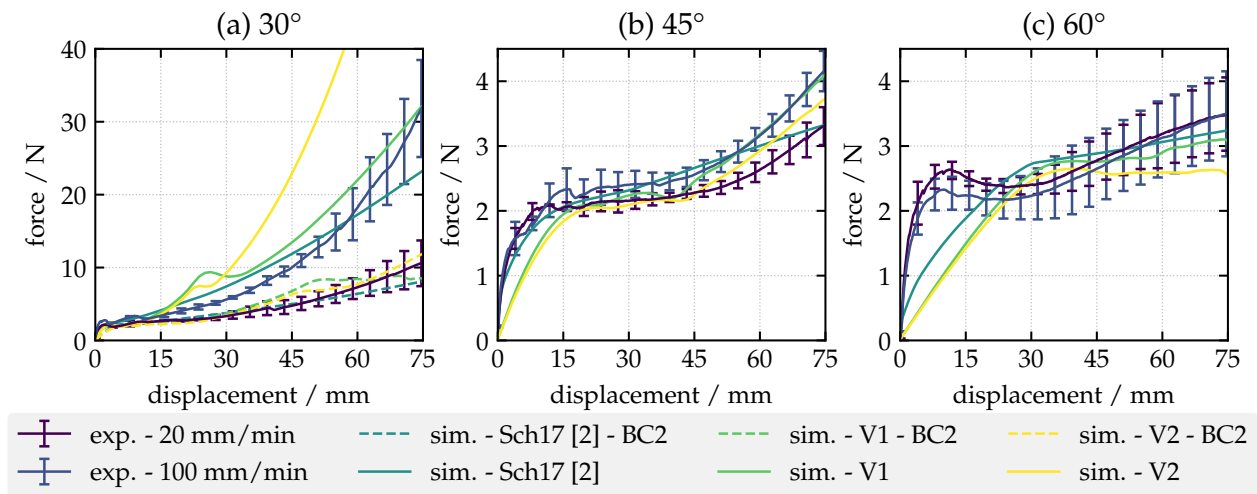

Fig. 3: Experimental and simulative force-displacement-curves for different fiber orientations (a) 30°, (b) 45° and (c) 60° (exp. curves based on [15])

Numerical Studies

The material parameters have been inversely identified by Schirmaier et al. [1,3] based on experimental off-axis-tension tests (OATs) of UD-NCF with three different orientations (30°, 45° & 60°). The experimental setups are shown in Figure 2a and the resulting force-displacement curves are shown in Figure 3. The OATs were conducted at two different velocities of 20 and 100 mm/min, while a square pattern of white points with a distance of $l_e = 10$ mm was applied to the front of the specimens for an optical strain measurement during the tests with 20 mm/min (cf. Fig. 4a). Unfortunately, during the 30°-OATs with the white square pattern, the carbon fibre bundles in the top right and bottom left edges of the specimens were slipping out of the clamping area. This resulted in significantly lower forces and presumably also smaller strains. The linear strain components, cf. Figure 1a, in the center of the specimens (green areas in Fig. 2a) were averaged and are shown in Figure 5.

The utilized simulation models with their respective boundary conditions are shown in 2b. Thereby, two sets of boundary conditions (BC) are used: BC 1 with all nodes in the clamping region fixed for simulation of the 30°-OATs with 100 mm/min; BC 2 with three free nodes in the clamping region to emulate the slipping of fibre bundles during the 30°-OATs with 20 mm/min. [1]. The results for the membrane model by Schirmaier et al. [1] are also shown in the respective Figures 3, 4 and 5. To compare the existing [1] and proposed hyperelastic membrane model, the chord-modulus $C_2^{\text{Sch17}}, C_\gamma^{\text{Sch17}}, C_\perp^{\text{Sch17}}$ between the origin and the resulting total stress-strain curves (elastic and yielding parts) for the different deformation modes is shown in Figure 6.
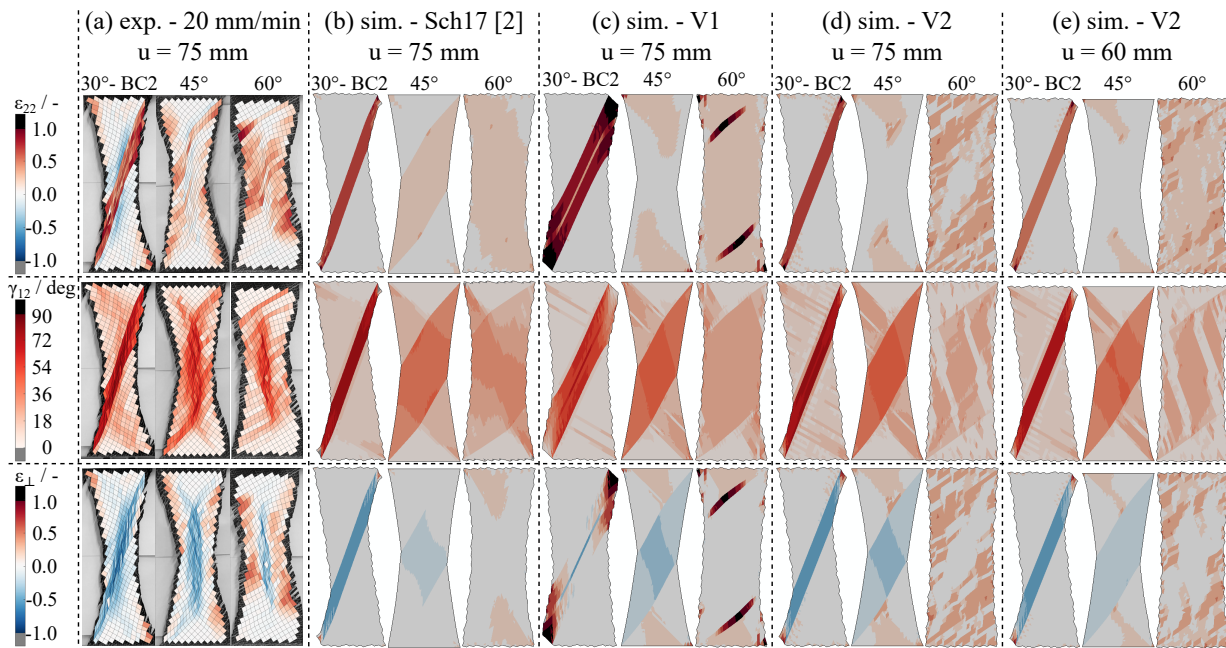

Fig. 4: Strain distributions of OATs with different orientations from (a) the experimental measurements (based on [1]), (b) the macroscopic model proposed by Schirmaier et al. [1] and (c-e) different parametrizations of the new membrane model

To investigate the new proposed membrane model, extensive numerical parameter studies have been conducted. Achieving an overall fit to all OATs with the reduced complexity of the new membrane model is complex, since the different orientations cause different multiaxial strain and thus stress conditions. Each nonlinear stiffness $C_2, C_\gamma, C_\perp$ influences the resulting forces and strains with varying intensity during different displacement ranges of the different orientations. In general, the perpendicular compressive stiffness $C_\perp$ mainly influences the strain distribution in the specimens as well as preventing a collapse of highly sheared elements, while only slightly impacting the forces. The tensile C_2 and shear C_γ stiffnesses on the other hand have a decisive influence on the force-displacement-relation for all orientations, while establishing the order of magnitude for the strains.

The initial stiffnesses C_2^{init} and C_γ^{init} determine the initial slopes and therefore resulting force-levels for the later course of the forces, which is especially relevant in the 45°- and 60°-OAT. The middle moduli C_2^{mid} and C_γ^{mid} mainly impact the later ranges of the 45°- ($u > 30$ mm) and 60°-OAT (> 40 mm), while having a significantly earlier impact for the 30°-OAT with BC1 ($u > 20$ mm). In the following, due to space limitations, only the results for two sets of parameters (V1 and V2) are shown to highlight some of the key findings and the remaining findings are summarized at the end of this section.
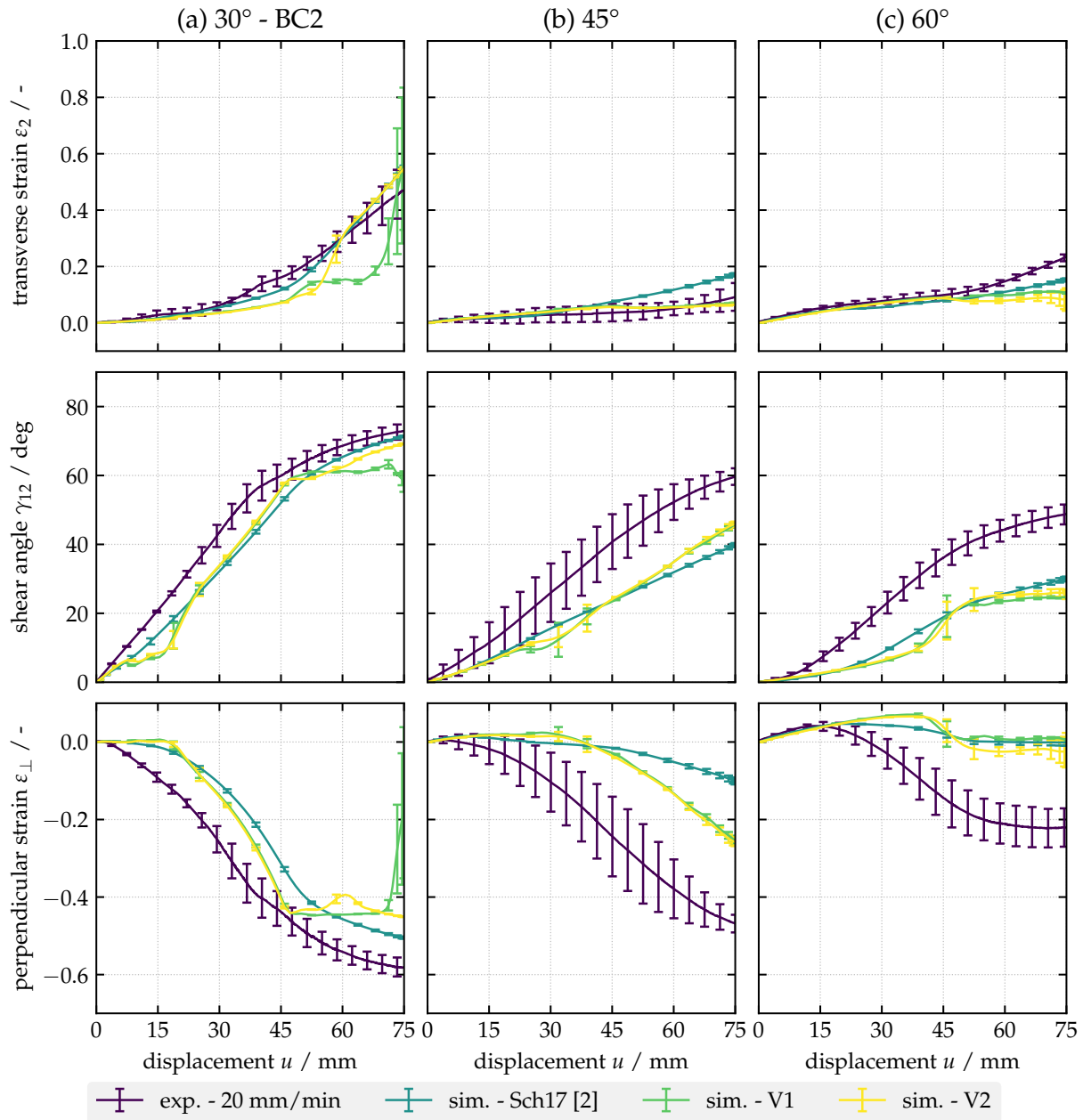

Fig. 5: Experimental and simulative strains in the specimen's center for different fiber orientations (a) 30° with slipping fibre in the clamping region - BC2, (b) 45° and (c) 60° (exp. curves based on [15])
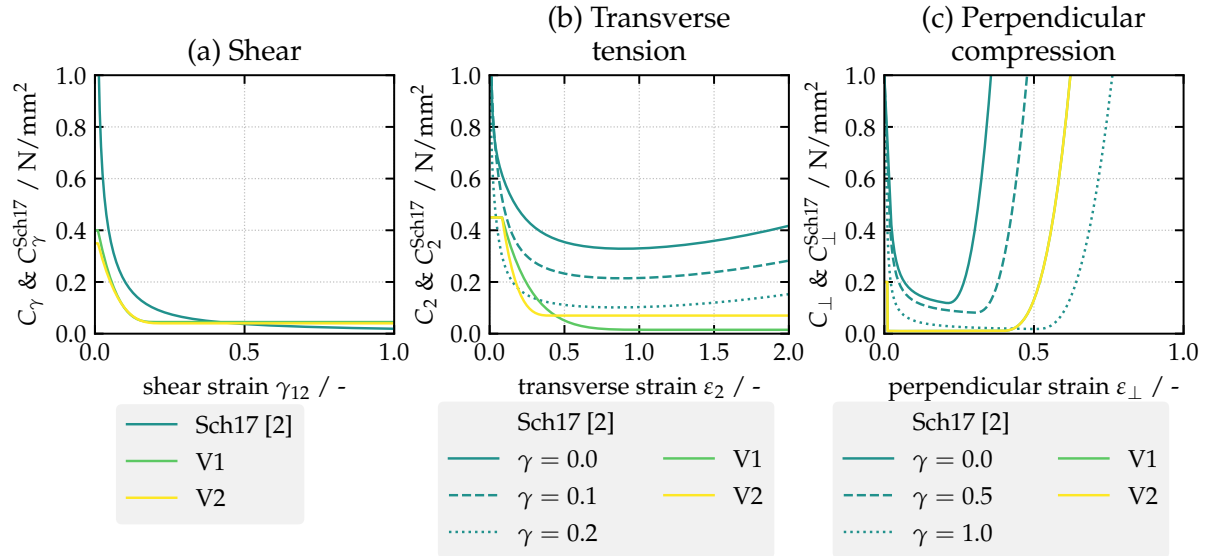
Fig. 6: Resulting stiffnesses of the model of Schirmaier el al. [1] represented by the chord modulus ($C_2^{\text{Sch17}}, C_\gamma^{\text{Sch17}}, C_\perp^{\text{Sch17}}$) between the origin and the total stress-strain curves and the nonlinear stiffnesses ($C_2, C_\gamma, C_\perp$) for the different deformation modes

Results for parameter set - V1. The first set of parameters was determined with the aim of achieving a good agreement for the force-displacement relation of the 30°-OAT with BC 1 as well as the 45°- and 60°-OAT (cf. Fig. 3). The initial steep force increase during the 45°- and 60°-OAT was underestimated compared to Sch17 [1] and the experimental results, but the steeper force increase during the 45°-OAT at a displacement > 40 mm was better predicted by the new model. However, the predicted force for the 30°-OAT was much higher compared to the experiments in the middle of the test (similar to Sch17 [1]). Additionally, a clear overshoot can be seen for a displacement between $23 - 32$ mm, which is caused by the steep decrease in the C_2-stiffness. This decrease is necessary, since the higher initial stiffness C_2^{init} is necessary to a achieve good agreement with the results of the 45°-OAT and 60°-OAT, but a significantly lower middle modulus C_2^{mid} is required to not severely overestimate the forces in the 30°-OAT.

The pure consideration of the force-displacement relation for the determination of the material parameters, however, leads to some problems with highly localized deformations when looking at the strain distributions (cf. Fig. 4c). Strongly localized tensile deformations ε_2 occur at the edge of the main deformation zone during the 60°-OAT and a general non-physical deformation of the central area in the 30°-OAT with BC2 with excessive tensile strains is visible. Nevertheless, the strain distributions of γ_{12} and $\varepsilon_\perp$ for the 45°-OAT tests seems comparable to the results from Sch17 [1] and the experimental results. Additionally, the averaged strains for all components are in the same range as the simulative results from Sch17 [1] or even closer to the experimental results for larger displacements during the 45°-OAT. A better overall agreement with the results of the 45°-OAT is achieved, because the deformation behaviour is shear dominated and only smaller tensile strains occur compared to the 30°- and 60°-OAT.

Results for parameter set - V2. Based on the evaluation of the first parameter set, a second set of parameters V2 was determined with the aim to alleviate the localised deformation during the 60°-OAT and 30°-BC2-OAT. Therefore, the strain range over which the tensile stiffness C_2 decreases was shortened (lower E_2^{mid}) and the middle modulus C_2^{mid} increased, while the shear stiffness C_γ was slightly reduced (cf. Fig. 6). The perpendicular compressive stiffness was not adjusted compared to parameter set V1.

The adaptations resulted in a similar overall fit to the forces in the 45°-OAT as for set V1 and only a small underestimation of the forces for higher displacements (> 45 mm) in the 60°-OAT (cf. Fig. 3). The predicted forces in the 30°-OAT are close to the experimental results for BC2, but significantly

overestimated compared to the experimental results for clamped fibre bundles in BC1 at an velocity of 100 mm/min. The examination of the global strain distributions shows, that the localized high tensile deformations ε_2 no longer occur (cf. Fig. 4). The strains during the 30°-BC2- and 45°-OAT are similar to the experimental as well as simulative results of Schirmaier et al. [1]. However, close to the clamping areas some positive tensile strains ε_2 occur that were not present during the simulations in Sch17 or the experiments.

The results for the 60°-OAT are significantly different from the simulative results in [1], but closer to the experimental results in some regions. The shear angle γ_{12} is more localized in a delimited area in the specimen's center and positive tensile ε_2 as well as perpendicular $\varepsilon_\perp$ strains are located around the main deformation zone in the specimen's center. This is similar to the experimental distribution in the lateral areas, but overestimated in the areas near the clamping. Additionally, at a global displacement of 60 mm an area with a slight perpendicular compression $\varepsilon_\perp$ is visible during the 60°-OAT, which is similarly oriented as in the experiment and was not predicted by the membrane model of Schirmaier et al. [1]. This compression in the central deformation zone during the 60°-OAT can also be seen regarding the averaged strains in Figure 5. Overall, the averaged strains (cf. Fig. 4) show a good agreement of the new model with the results of Schirmaier el al. The simulative strains in the 45°-OAT are closer to the experimental results compared to Schirmaier el al., but deviate slightly more from them for large displacements in the 30°-OAT for BC2.

Further results of the numerical studies. During the numerical parameter studies, some additional findings were made which are not shown due to space limitations, but which are summarized in the following:

- The locking parts for the shear $E_{12} > E_\gamma^{\text{lock}}$ and tensile $E_{22} > E_\gamma^{\text{lock}}$ stiffness are not utilized in this work, since their introduction always led to a clear overestimation of the forces. A variation of the parameters relevant for locking in the yield surface $R_{2,\Gamma}(\varepsilon_{2,\text{p}}, \gamma_{12})$ and yield curve $R_{12,\Gamma}(\gamma_{12,\text{p}})$ of Schirmaier et al.'s membrane model [1] resulted in similar observations. The shear locking in their model occurred in a strain range, that was not relevant for the OATs and the tensile locking was hardly pronounced, such that the slope in the resulting stiffness barely deviated from that in the medium strain range.
- The introduction of a perpendicular compressive locking $E_\perp > E_\perp^{\text{lock}}$ was required to prevent a collapse of highly sheared elements. However, coupling the behaviour to the shear angle was not necessary for a simulation of the OATs.
- The approach is susceptible to numerical instabilities if the ratio between the initial ($C_\perp^{\text{init}}/C_2^{\text{init}}$) or middle ($C_\perp^{\text{mid}}/C_2^{\text{mid}}$) moduli is high
- In order to parametrize the model to account for the different multiaxial strain conditions of the OATs, a pure focus on the force-displacement relations is not sufficient and the strain distributions must be taken into account.
- The behaviour during the 45°-OAT is mostly dominated by shear deformation, compared to the 30°- and 60°-OAT in which proportionally a higher amount of transverse tensile deformation occurs. Therefore, the transverse tensile stiffness $C_2(E_2)$ is the most suitable for adapting the membrane model to the different orientations in the OATs after a rough initial shear stiffness has been determined. Thereby, it turned out that an uncoupled transverse tensile behaviour is not sufficient to achieve a satisfactory overall fit.

Conclusion and Outlook

A new model for the membrane behaviour of UD-NCF based on superimposed shear, transverse tensile and perpendicular to the carbon fiber tows oriented compressive strains is presented. The approach uses similar principles as the detailed model presented by Schirmaier et al. [1], but introduces several simplifications to investigate what level of complexity is necessary. Two parametrizations are presented to highlight some of the key findings, each of which required a total of 18 model parameters

(C_1, five for $C_2(E_{22})$ and $C_\gamma(E_{12})$ without locking, seven for $C_\perp(E_\perp)$) compared to 49 parameters in [1]. The first variant (V1) with the material parameters fitted to predict the force-displacement relation of the OATs at 100 mm/min, was used to show that both the resulting forces and strains must be considered to determine the material stiffnesses. The second variant (V2) with adapted material parameters to prevent localised deformations observed during V1, achieved a similarly good agreement with the resulting experimental strains as the detailed model from [1] (cf. Fig. 4 and 5). However, the forces in the 60°-OAT were slightly underestimated and in the 30°-OAT without slipping carbon fibre bundles considerably overestimated.

The numerical investigations suggest that with the proposed principle strain directions, shear and transverse tensile locking have no or at most a minor relevance for the loading conditions tested within the different OATs, while a perpendicular compressive locking was necessary. A coupling between the perpendicular compressive and shear behaviour is not required. However, a coupling between the transverse tensile stiffness and the shear strains will be necessary in future work. This is indicated by the observation, that in the 30°-OAT the force is clearly overestimated due to the increased C_2^{mid} from V1 to V2, while the forces in the 60°-OAT are still underestimated. Therefore, a decreasing transverse tensile stiffness for higher shear deformations seems to be required to model the behaviour properly

Additionally, it must be investigated whether neglecting the coupling of the transverse compressive and shear behaviour has an influence on the occurrence of wrinkles perpendicular to the fibre directions as proposed by Schirmaier et al. [1]. Meanwhile, it will also be necessary to investigate the influence of a purely hyperelastic membrane model compared to an elastic-plastic approach during component forming simulations.

Acknowledgements

References

[1] F. J. Schirmaier, D. Dörr, F. Henning, and L. Kärger, *A macroscopic approach to simulate the forming behaviour of stitched unidirectional non-crimp fabrics (UD-NCF)*, Composites Part A: Applied Science and Manufacturing, (2017), pp. 322–335.

[2] S. Galkin, E. Kunze, L. Kärger, R. Böhm, and M. Gude, *Experimental and Numerical Determination of the Local Fiber Volume Content of Unidirectional Non-Crimp Fabrics with Forming Effects*, Journal of Composites Science, 3 (2019).

[3] F. J. Schirmaier, K. A. Weidenmann, L. Kärger, and F. Henning, *Characterisation of the draping behaviour of unidirectional non-crimp fabrics (UD-NCF)*, Composites Part A: Applied Science and Manufacturing, 80 (2016), pp. 28–38.

[4] E. Kunze, S. Galkin, R. Böhm, M. Gude, and L. Kärger, *The Impact of Draping Effects on the Stiffness and Failure Behavior of Unidirectional Non-Crimp Fabric Fiber Reinforced Composites*, Materials (Basel, Switzerland), 13 (2020).

[5] P. Bussetta and N. Correia, *Numerical forming of continuous fibre reinforced composite material: A review*, Composites Part A: Applied Science and Manufacturing, 113 (2018), pp. 12–31.

[6]   B. Liang and P. Boisse, *A review of numerical analyses and experimental characterization methods for forming of textile reinforcements*, Chinese Journal of Aeronautics, (2020).

[7]   G. Creech and A. Pickett, *Meso-modelling of Non-Crimp Fabric composites for coupled drape and failure analysis*, Journal of Materials Science, 41 (2006), pp. 6725–6736.

[8]   S. Lomov, D. Ivanov, I. Verpoest, M. Zako, T. Kurashiki, H. Nakai, and S. Hirosawa, *Meso-FE modelling of textile composites: Road map, data flow and algorithms*, Composites Science and Technology, 67 (2007), pp. 1870–1891.

[9]   J. Sirtautas, A. K. Pickett, and P. Lépicier, *A mesoscopic model for coupled drape-infusion simulation of biaxial Non-Crimp Fabric*, Composites Part B: Engineering, 47 (2013), pp. 48–57.

[10] A. Mallach, F. Härtel, F. Heieck, J.-P. Fuhr, P. Middendorf, and M. Gude, *Experimental comparison of a macroscopic draping simulation for dry non-crimp fabric preforming on a complex geometry by means of optical measurement*, Journal of Composite Materials, 51 (2017), pp. 2363–2375.

[11] P. Böhler, F. Härtel, and P. Middendorf, *Identification of Forming Limits for Unidirectional Carbon Textiles in Reality and Mesoscopic Simulation*, Key Engineering Materials, 554-557 (2013), pp. 423–432.

[12] T. Senner, S. Kreissl, M. Merklein, J. Meinhardt, and A. Lipp, *A modular modeling approach for describing the in-plane forming behavior of unidirectional non-crimp-fabrics*, Production Engineering, 8 (2014), pp. 635–643.

[13] C. Krogh, J. A. Kepler, and J. Jakobsen, *Pure and simple: investigating the in-plane shear kinematics of a quasi-unidirectional glass fiber non-crimp fabric using the bias-extension test*, International Journal of Material Forming, 19 (2021), pp. 1483–1495.

[14] L. Kärger, S. Galkin, E. Kunze, M. Gude, and B. Schäfer, *Prediction of forming effects in UD-NCF by macroscopic forming simulation – Capabilities and limitations*, ESAFORM 2021, (2021).

[15] F. Schirmaier, *Experimentelle Untersuchung und Simulation des Umformverhaltens nähgewirkter unidirektionaler Kohlenstofffasergelege*, PhD thesis (in German), Karlsruher Institute for Technology, Karlsruhe, Germany, 2017.

[16] C. Poppe, D. Dörr, F. Henning, and L. Kärger, *Experimental and numerical investigation of the shear behaviour of infiltrated woven fabrics*, Composites Part A: Applied Science and Manufacturing, 114 (2018), pp. 327–337.

[17] G. A. Holzapfel, *Nonlinear Solid Mechanics: A Continuum Approch for Engineering*, John Wiley & Sons Lt., West Sussex, England, 2000.